Effect of nitrogen-doping temperature on the structure and photocatalytic activity of the B,N-doped TiO$_2$

Xiaosong Zhou, Feng Peng*, Hongjuan Wang, Hao Yu, Jian Yang

School of Chemistry and Chemical Engineering, South China University of Technology, Guangzhou 510640, PR China

ABSTRACT

B,N-TiO$_2$ photocatalysts were synthesized by boron doping firstly and subsequently nitrogen doping in NH$_3$ at variable temperatures. The effects of the nitrogen doping temperature on the structure and photocatalytic activity of the B,N-codoped TiO$_2$ were investigated. The as-prepared samples were characterized by X-ray diffraction (XRD), scanning electron microscopy (SEM), UV–vis diffuse reflectance spectrum (DRS), electron paramagnetic resonance (EPR) and X-ray photoelectron spectroscopy (XPS). The photocatalytic activity was evaluated with photocatalytic degradation of methyl orange dye (MO) under visible light and UV–visible light irradiation. The results suggested that the boron and nitrogen can be incorporated into the TiO$_2$ lattice either interstitially or substitutionally or both, while the Ti–O–B–N structure plays a vital role in photocatalytic activity in visible light region. The optimal nitrogen doping temperature is 550 °C. Higher temperature may form many oxygen vacancies and Ti^{3+} species, resulting in the decrease of photocatalytic activity in visible light.

© 2010 Elsevier Inc. All rights reserved.

1. Introduction

Since Asahi et al. [1] showed that nitrogen doping significantly improved the photocatalytic reactivity of TiO$_2$ in the visible light region, they opened a new way to decrease the photothreshold energy of TiO$_2$. Extensive efforts have been made in TiO$_2$ doping with non-metal ions, such as B, C, N and S [2–5]. TiO$_2$ doping with these non-metal ions showed good photocatalytic activity under visible light. Recently, many groups reported that codoped materials, such as F and N [6,7], S and N [8,9], C and N [10,11] and N and a variety of metal ions [12–14], can extend the photocatalytic activity of TiO$_2$ into the visible-light region. Especially, the B,N-codoped titania has been considered as the most effective approach to improve photocatalytic activity in visible region [15–17]. However, some important issues about the B,N-codoped TiO$_2$ photocatalyst still remain unclear. The issues include the following: (1) what is the intrinsic catalytic mechanism in visible light? Cheng et al. proposed that the nitrogen substitution for oxygen and the resultant oxygen vacancies in the titania matrix improved its visible-light absorption. The high photocatalytic activity under visible light irradiation might be aroused by O–Ti–B–N or Ti–O–B–N structure [16,17]. However, In et al. [15] showed the absence of the synergistic effect by B and N doping. (2) Does nitrogen and boron co-doping induce other defect states like Ti^{3+} in the band gap that is usually associated with oxygen vacancies?

Here, B-doped TiO$_2$ was synthesized firstly and then followed with nitrogen doping. The effects of the nitrogen doping temperature on the structure and photocatalytic activity of the B,N-codoped TiO$_2$ were investigated. The catalyst showed high photocatalytic activity in the degradation of MO under visible light irradiation, when the nitrogen doping temperature was set at 550 °C. Many techniques were taken to investigate the chemical and structure features of the prepared catalysts. Especially, X-ray photoelectron spectroscopy (XPS) and electron paramagnetic resonance (EPR) were used to reveal the origin of the visible light absorption properties and the photo-activity of the boron and nitrogen doped TiO$_2$ catalyst. The results show that the synergistic effect of interstitial boron and nitrogen acts as a key role in photocatalytic activity.

2. Experimental

2.1. Synthesis of boron and nitrogen-codoped titanium dioxide

The boron doped titanium dioxide was prepared as the reference [16]. In a typical preparation experiment, the mixture solution of Ti[OCH(CH$_3$)$_2$]$_4$ (5 mL, Aldrich, 97%) and isopropyl alcohol (40 mL, J&K CHEMICA, 98%) were added dropwise into a solution of HNO$_3$ (50 mL, pH=1.0) containing a known amount of boric acid. After aging for 10 h at room temperature, the mixture was hydrothermally treated at 85 °C for 5 h. Then the gel was added dropwise into 20 mL aqueous solution (10 wt%) of the block copolymer Pluronic P123 (EO$_{20}$PO$_{70}$EO$_{20}$) at 40 °C and stirred

---

* Corresponding author. Fax: +86 20 87114916.
  E-mail address: cefpeng@scut.edu.cn (F. Peng).

vigorously for 2 h. The mixture was hydrothermally treated again at 110 °C for 20 h. The resultant gel was dried at 200 °C for 10 h and then was calcined at 400 °C for 2 h in air to obtain B-TiO$_2$. This sample was further annealed at variable temperatures under an ammonia atmosphere to synthesize B,N-codoped TiO$_2$, which was denoted as B,N-TiO$_2$-X (X denotes doping temperature).

2.2. Characterization of catalysts

The crystal structure of samples was characterized by powder X-ray diffraction (XRD) on an X-ray diffractometer (D/max-IIIA, Japan) using CuKα radiation and operating at 30 kV/30 mA at the angle range 10–80°. The morphology of the catalyst was characterized by transmission electron microscopy (TEM, JEOL, JEM2010) with the instrument operating at 200 kV. The UV–vis light absorption spectra were obtained from a Hitachi UV-3010 spectrophotometer equipped with an integrating sphere assembly. The diffuse reflection method and BaSO$_4$ as a reference were used to measure all the samples. The Brunauer–Emmett–Teller surface area (S_{BET}) of the samples was determined by nitrogen adsorption–desorption isotherm measurements at 77 K on a Micromeritics ASAP 2010 system. The samples were degassed in vacuum at 473 K until the pressure was lower than 10^{-6} Torr before the actual measurements. The chemical nature of boron and nitrogen in TiO$_2$ was studied using X-ray photoelectron spectroscopy in Krato Axis Ultra DLD spectrometer with AlKα X-ray ($h\nu = 1486.6$ eV) at 15 kV and 150 W. The binding energy was referenced to C 1s line at 284.9 eV for calibration. The paramagnetic species of nitrogen in the as-synthesized B,N-TiO$_2$ photocatalysts were measured on a Bruker A300 electron paramagnetic resonance spectrometer. Instrument settings are as follows: microwave frequency of 9.51 GHz; microwave power of 3.16 mW and modulation amplitude of 1 G at 100 kHz.

2.3. Photocatalytic reaction

The photocatalytic reaction was conducted in a 200 mL cylindrical glass vessel fixed in the XPA-II photochemical reactor (Nanjing Xujiang Machine-electronic Plant). A 500 W Xe lamp was used as the simulated solar light source (UV–visible light) and a home-made filter was mounted on the lamp to eliminate infrared irradiation. The cut-off filter was made up of 1 M sodium nitrite solution that can absorb the light with wavelength under 400 nm [18]. This solution was injected into the interlayer of the quartz cool trap to be used as filter, which was placed after the water filter to completely remove the UV portion of the radiation and to supply a visible-light source. Methyl orange (MO) dye with the concentration of 20 mg/L was used as contamination. In order to obtain an optimally dispersed system and reach complete adsorption/desorption equilibration, 20 mg photocatalyst powder was dispersed in 200 mL reaction solutions by ultrasonicating for 15 min, and then the suspension was magnetically stirred in dark for 1 h. During the photocatalytic reaction, air was added into the reaction medium at a flow rate of 200 mL/min. At regular intervals, 8 mL of the suspension was sampled and filtered through a 0.2 μm membrane filter. The concentration of the remaining MO was measured by its absorbance (A) at 465 nm with a Hitachi UV-3010 spectrophotometer. The degradation ratio of MO can be calculated by $(A_0 - A)/A_0 \times 100\%$.

2.4. Photoluminescence measurement

The terephthalic acid (C$_8$H$_6$O$_4$, TA) can be used to confirm the existence of ˙OH by a fluorescent method, since ˙OH reacts with TA and generates luminescent TAOH as shown in Eq. (1) [19,20]:

$$\text{˙OH} + \text{TA} \rightarrow \text{TAOH} \qquad (1)$$

50 mg of as-prepared photocatalyst was added to 160 mL of solution containing 10 mM NaOH and 3 mM TA in a quartz reactor. Prior to photoreaction, the suspension was magnetically stirred in the dark for 1 h to ensure the establishment of an adsorption/desorption equilibrium. The photoreaction was carried out as the foregoing photocatalytic reaction under UV–visible light without oxygen bubbled into suspension. After photoreaction of 2 h, 8 mL suspension was collected, filtered and centrifuged to remove the photocatalyst particles. Photoluminescence (PL) spectra were measured with a fluorospectrophotometer (SPEX Fluoromax-2) using a Xe lamp as the excitation source at room temperature. Equally weighed powder samples dissolved in terephthalic acid solution were used for PL measurements. The employed excitation light for recording fluorescence spectra was 320 nm. The entrance and exit slit widths were kept the same.

3. Results and discussion

3.1. Crystal structure

Fig. 1 reveals XRD patterns of the as-synthesized products of B,N-TiO$_2$-X and B-TiO$_2$. All samples show pure anatase phase except for B,N-TiO$_2$-650 that contains both anatase and rutile due to the effect of annealing temperature. There are no boron- and nitrogen-derived peaks in the XRD pattern, because the content of boron and nitrogen is well below the detection limit of XRD. Thus, B and N dopings do not cause the change in crystallite of TiO$_2$. The anatase crystal sizes were calculated by the Scherrer equation. As shown in Table 1, the BET specific surface areas decreases and the nitrogen contents increases with the increase of treatment temperatures.

Fig. 2 shows the TEM images of B-TiO$_2$ and B,N-TiO$_2$-550. In Fig. 2a, the B-TiO$_2$ particles exhibit an irregular shape with the size range from 7 to 14 nm and the mean size of about 11 nm. After annealed in ammonia atmosphere, the mean size of B,N-TiO$_2$-550 particles is 10 nm, as shown in Fig. 2b, which is consistent with its XRD result (9.3 nm). It suggests the particle size and morphology do not change remarkably after nitrogen doping in ammonia atmosphere.
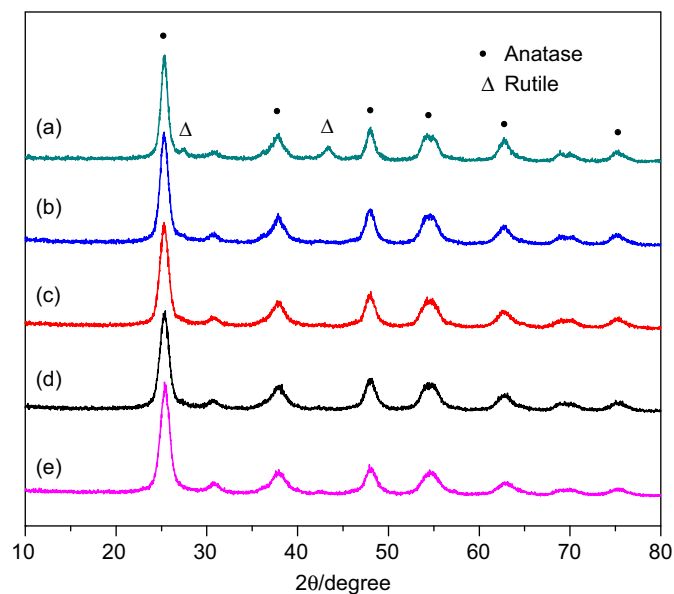

Fig. 1. XRD patterns of B,N-TiO$_2$ samples: (a) B,N-TiO$_2$-650; (b) B,N-TiO$_2$-600; (c) B,N-TiO$_2$-550; (d) B,N-TiO$_2$-500 and (e) B-TiO$_2$.

3.2. XPS analysis

The chemical states of boron and nitrogen dopants in the titania surface was investigated by high-resolution XPS, as shown in Fig. 3. It can be seen from Fig. 3(1) that B 1s core level peaks of the as-prepared B-doped TiO_2 appear at around 192.6 and 191.4 eV, which are attributed to Ti–O–B and Ti–B bonds [21] as interstitial and substitutional boron, respectively. After annealed under NH_3 flow, a new peak with its center at 190.6 eV appears in the B 1s spectrum of B,N-codoped TiO_2, which is attributed to B–N bond [17], indicating Ti–O–B–N bond or Ti–B–N bond are formed. While the peak corresponding to the Ti–B bond shifts from 191.4 to 191.8 eV due to the nitrogen doping.

The spectra of N 1s for B, N codoped TiO_2 are shown in Fig. 3(2), we can sort the binding energies (BE) of N1s into three ranges: 400.5, 398.0–398.9 and 396.4 eV. As reported earlier [22–25], we attribute the core level N1s peak at around 400 eV to oxidized nitrogen in the form of Ti–O–N linkage as interstitial nitrogen, and the core level N1s peak at around 396.4 eV to Ti–N linkage as substitutional nitrogen. According to the literatures [16,17], the core level N 1s peak at around 398.0–398.9 eV may be originated from Ti–O–B–N bond.

Fig. 4(1) reveals the O 1s spectra of B,N-TiO_2-550. Oxygen 1s core level peaks appear at 532.8, 530.4 and 528.3 eV. The peak at 530.4 eV is the intrinsic peak of Ti–O–Ti linkage in TiO_2, which is consistent with that of most reported ones [26,27]. We attribute the O 1s peak at 528.3 eV to Ti–O–N [28] or Ti–O–B [21] linkage in B,N-TiO_2. In addition, in view of O 1s peak of –NO and –NO_2 at 533.5 eV [24], the peak at 532.8 eV can be attributed to the presence of the oxygen from NO_X, due to the N interstitially doping into the TiO_2 lattice, which agrees with the result of N 1s XPS.

Usually, the Ti $2p_{3/2}$ and $2p_{1/2}$ peaks at 458.9 and 464.7 eV which are attributed to the Ti 2p peaks of O–Ti–O in TiO_2 [26,29]. It is clear to see that two couples of different Ti peaks are observed in

Table 1
Anatase crystal size, the N content and BET of B,N-TiO_2.

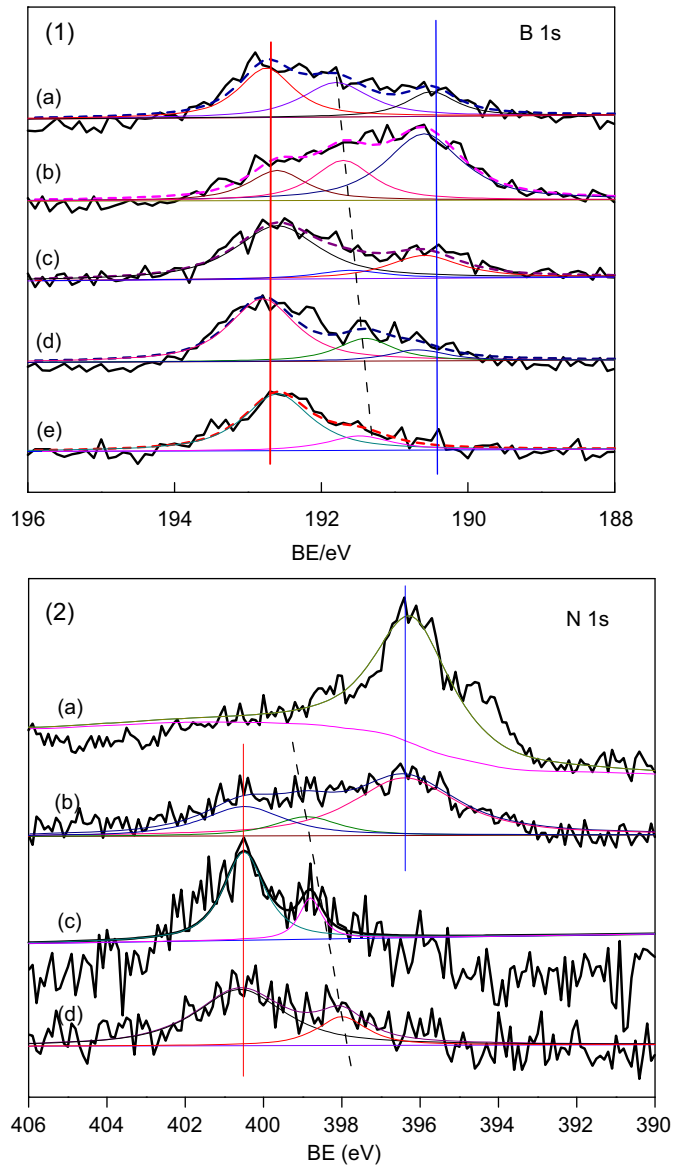| Sample	N content (at%)	Anatase crystal size (nm)	BET (m²/g)
BN500	1.28	8.6	169.6
BN550	1.35	9.3	163.0
BN600	1.94	9.8	149.4
BN650	2.91	10.3	135.9

Fig. 3. XPS spectra for (1) B 1s and (2) N 1s core levels of B,N-TiO_2 samples: (a)B,N-TiO_2-650; (b) B,N-TiO_2-600; (c) B,N-TiO_2-550; (d) B,N-TiO_2-500 and (e) B-TiO_2.
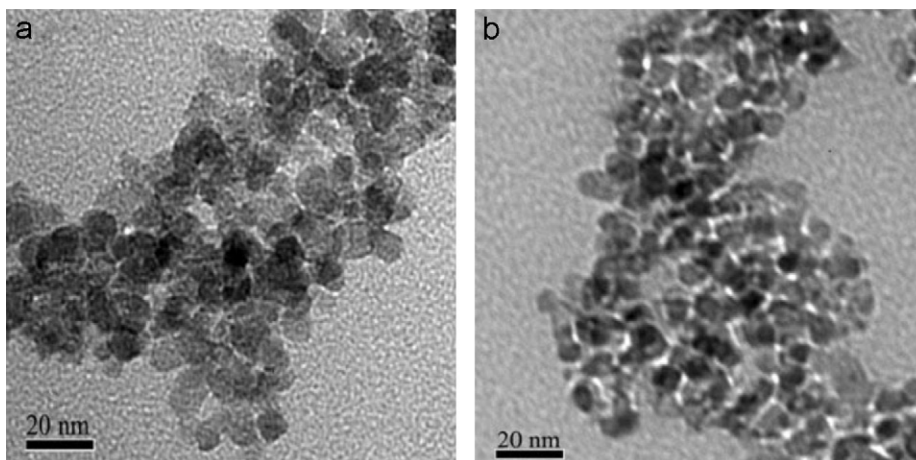

Fig. 2. TEM patters of samples: (a)B-TiO_2 and (b) B,N-TiO_2-550.
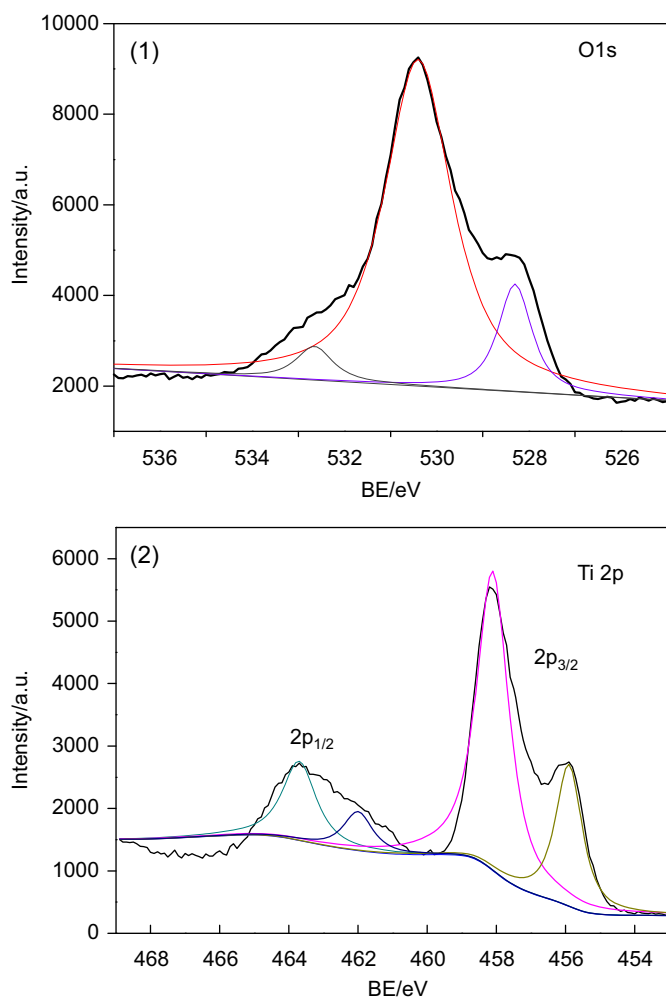
Fig. 4. XPS spectra for (1) O 1s and (2) Ti 2p core levels of B,N-TiO$_2$-550.

Fig. 5. EPR spectra of B,N-TiO$_2$ samples: (a) B,N-TiO$_2$-650; (b) B,N-TiO$_2$-600; (c) B,N-TiO$_2$-550 and (d) B,N-TiO$_2$-500.

Fig. 6. UV–vis absorption spectra of B,N-TiO$_2$ samples: (a) B,N-TiO$_2$-650; (b) B,N-TiO$_2$-600; (c) B,N-TiO$_2$-550; (d) B,N-TiO$_2$-500 and (e) B-TiO$_2$.

B,N-TiO$_2$-550, as shown in Fig. 4(2). The main pair of peaks appears at 458.2 and 463.7 eV, which can be assigned to Ti 2p peaks of Ti–O–N and Ti–O–B in B,N-TiO$_2$. It needs to be noted that the binding energy of the Ti 2$p_{3/2}$ and 2$p_{1/2}$ peaks of this main pair shifts to lower energies by 0.7 and 1.0 eV compared with TiO$_2$. Most of the reports agreed on the lower BE of Ti 2p in doped TiO$_2$ [26,29]. Another pair of Ti 2$p_{3/2}$ and 2$p_{1/2}$ core level peaks appears at 455.9 and 462.0 eV, which can be attributed to N-Ti [31] or B-Ti in B,N-TiO$_2$. The BE of the Ti 2$p_{3/2}$ and 2$p_{1/2}$ peaks shifts to even lower energies by 2.7 and 3.0 eV compared with pure TiO$_2$. This suggests that partial Ti^{4+} is partially reduced to Ti^{3+} in B,N-TiO$_2$-550.

3.3. EPR and UV–vis absorption spectra analysis

Fig. 5 shows the EPR spectra of the B,N-TiO$_2$ catalysts obtained at different N-doping temperatures. The paramagnetic N species are observed mainly in B,N-TiO$_2$ with the doping temperature range 500–600 °C. The corresponding values of g_1, g_2 and g_3 are 2.006, 2.005 and 2.004, respectively. According to EPR results and theoretical modeling, they are assigned to a species containing a nitrogen atom trapped in TiO$_2$ lattice or in the bulk of TiO$_2$ [32]. However, the features of these N species are ambiguous at present in all the reported EPR spectra. A conclusive judgement on the N atom site (substitutional or interstitial N atom) in TiO$_2$ structure cannot be totally made [32]. We can see that the intensities of the signals for paramagnetic N species at the doping temperature of 600 °C are much lower than those of the others and some new
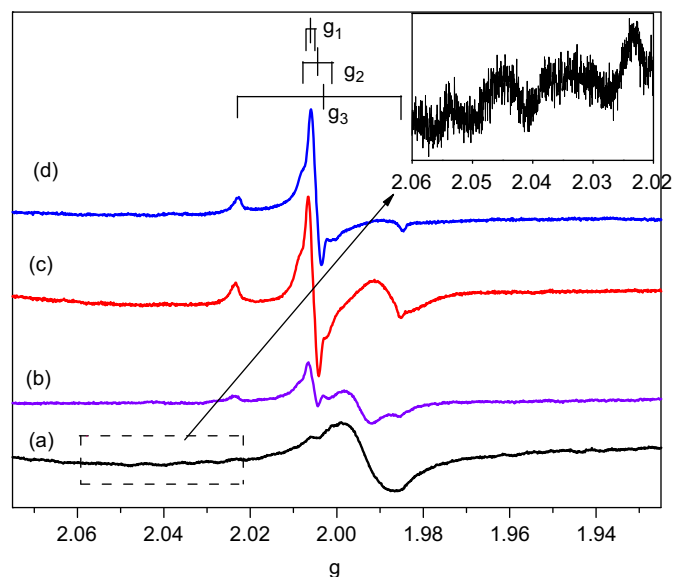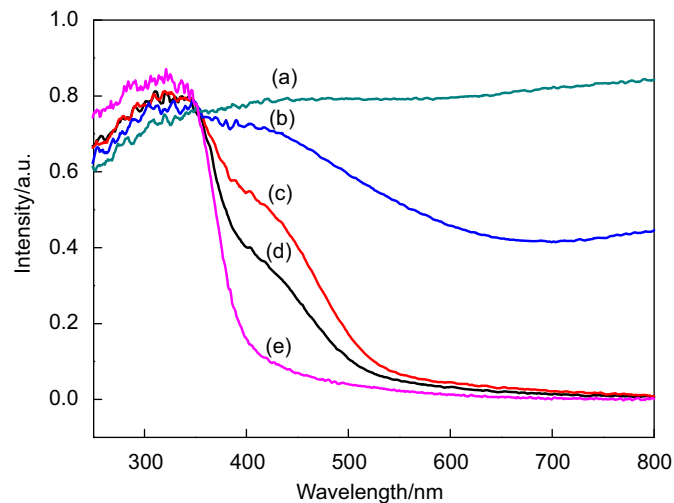
peaks appear for this sample. For B,N-TiO$_2$-650, the g-values of new peaks are between 1.985 and 1.999, which are attributed to Ti^{3+} species [33,34]. The curve shows a composite resonance arising from both surface and bulk Ti^{3+} centers of BN-TiO$_2$-650, which agrees well with the results of XPS. Since boron is diamagnetic in B-doped anatase TiO$_2$ nanoparticles, the substitutional boron in an oxygen vacancy in B-TiO$_2$ is EPR silent [33]. Gopal et al. [33] reported that B,N-TiO$_2$ exhibited two sets of nitrogen based EPR signals. The first set of signals, identical to that for g-values 2.006–2.004, is due to isolated N centers in B,N-TiO$_2$. The second set of signals is an indication that a nitrogen based center interacts with boron nucleus. This interaction causes the nitrogen hyperfine signal to further split into a quartet and this nitrogen based center is designated as a "B coupled N-center". In our work, the EPR spectra of as-prepared B,N-TiO$_2$-650 are similar to those of the reported ones. The second set of signals for the nitrogen hyperfine quartet is shown in Fig. 5 inset, which indicates boron nucleus and nitrogen nucleus are tied tightly to each other.

Fig. 6 gives the UV–visible absorption spectra of the as-prepared B-TiO$_2$ and B,N-TiO$_2$. For the B,N-TiO$_2$-500 and B,N-TiO$_2$-550,

an add-on shoulder peak is imposed onto the cutoff edge of the absorption spectrum, which enhances the visible light absorption. The absorbance intensity in the visible light range increases with the increase of the temperatures of nitrogen doping. Such light absorbance enhancement in the near-UV region and in the visible light range is consistent with the dark green and black color characteristic of B,N-TiO$_2$-600 and B,N-TiO$_2$-650.

3.4. Photocatalytic activity

Fig. 7 shows the photocatalytic activity of the as-prepared B,N-TiO$_2$ nanoparticles in the degradation of MO under both UV–visible and visible irradiation. Under visible-light irradiation (Fig. 7(1)), the photocatalytic activity of B,N-TiO$_2$ increases first with the increase of nitrogen-doping temperatures and then decreases with the further increase of the temperatures. The B,N-TiO$_2$-550 catalyst exhibits the highest photocatalytic activity that is almost doubled compared with B,N-TiO$_2$-500 or B,N-TiO$_2$-600. While B,N-TiO$_2$-650 only preserves a little activity. Under the irradiation of UV–visible light (Fig. 7(2)), the similar result is observed. The B,N-TiO$_2$-550 catalyst also exhibits the highest photocatalytic activity. However, it should be pointed out that the photocatalytic activity of B,N-TiO$_2$-650 is higher than that of B,N-TiO$_2$-600 in this case. All these

results reveal the effect of N-doping temperature on the photo-catalytic performance.

Since TA reacts with $\cdot$OH and gives highly luminescent TAOH, TA is used as a sensitive probe for the detection of $\cdot$OH. The emission band at 430 nm that originates from TAOH present the amount of $\cdot$OH produced by B,N-TiO$_2$ under the UV–visible light. As shown in Fig. 8, the fluorescent intensity of the catalysts obtained at different N-doping temperature is B,N-TiO$_2$-550 > B,N-TiO$_2$-500 > B,N-TiO$_2$-650 > B,N-TiO$_2$-600, which is in good agreement with the degradation ratio under the UV–visible light. The TA probe confirms that the photogenerated holes left in the valence band of B,N-TiO$_2$ can oxidize hydroxyl to give $\cdot$OH under the UV–visible light.

3.5. Discussion

Based on the above analysis and results, it is clear to see that temperature of nitrogen doping plays an important role in the structure and activity of the prepared photocatalyst. Under nearly the same conditions, such as morphology, particle size and specific surface area conditions (Fig. 2 and Table 1), we think that the changes of photocatalytic activity of B,N-TiO$_2$ with variable nitrogen doping temperatures are attributed to B–N structure and oxygen vacancy. Firstly, because the oxygen vacancies give rise to the local states below the conduction edge and the interstitial nitrogen atoms induce the local states near the valence band edge, both the doped atoms and the oxygen vacancies in the lattice of TiO$_2$ can extend its light absorption from UV to visible range. The "add-on shoulder peak" on the absorption edge of the UV–visible spectrum for B,N-TiO$_2$ at N doping temperatures of 500 and 550 °C is consistent with the excitation from the local states near the valence band edge to the conduction band. Ammonia gas usually decomposes to H$_2$ and N$_2$ gas at about 550 °C [35], which may partially reduce Ti^{4+}–Ti^{3+}. Recently, Serpone [36] proposed that oxygen vacancies induced by anion doping in TiO$_2$ could act as the color center. Furthermore, the electrons departed from the oxygen vacancies can interact with adjacent Ti^{4+} to give the Ti^{3+} color center, which in titania also contributes to the visible light absorption of titania. According to these, with higher N doping temperature, the higher N dopant content will lead to more oxygen vacancies. Thus, the absorbance intensity of B,N-TiO$_2$ in visible light range increases with the increase of nitrogen doping temperatures.
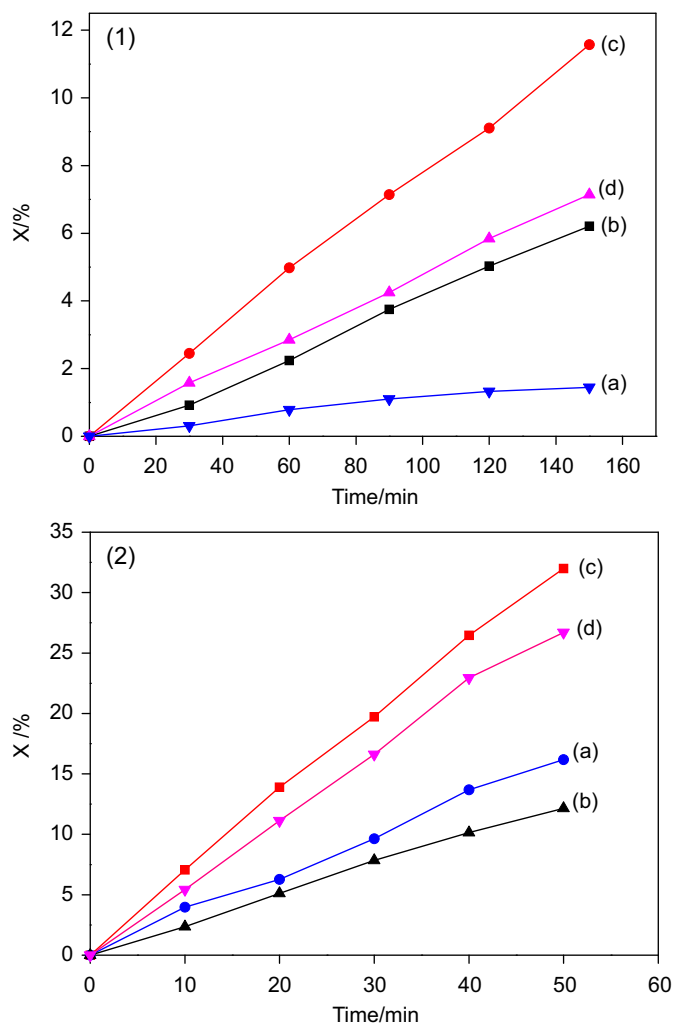

Fig. 7. Photocatalytic activity for decomposition of methyl orange under (1) visible light and (2) UV–visible light irradiation: (a) B,N-TiO$_2$-650; (b) B,N-TiO$_2$-600; (c) B,N-TiO$_2$-550 and (d) B,N-TiO$_2$-500.
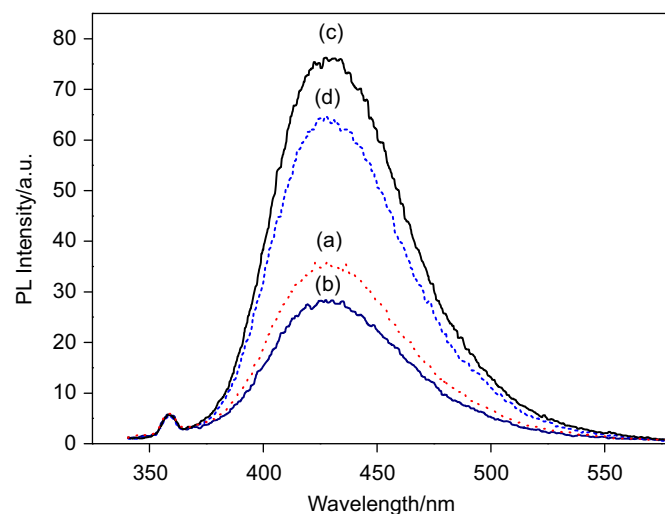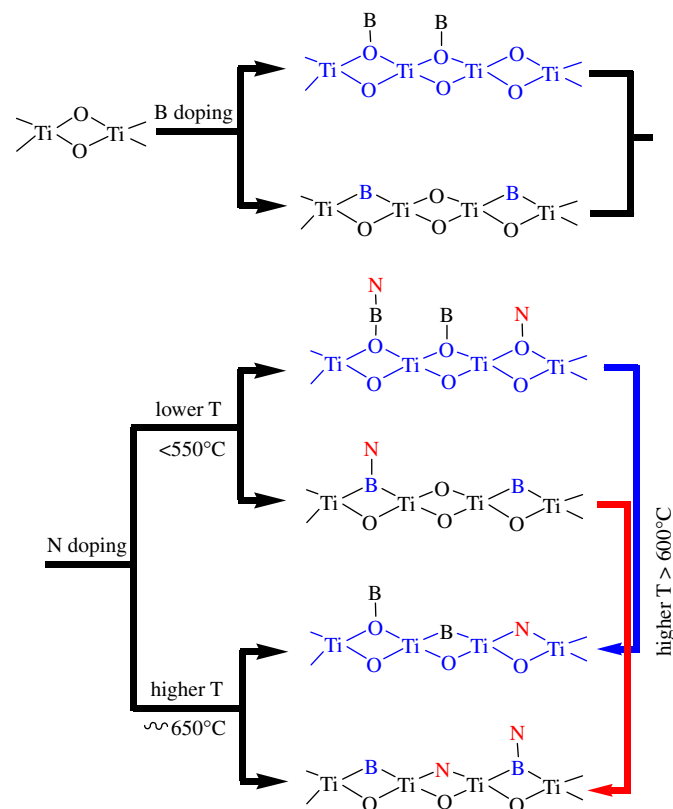

Fig. 8. Fluorescence spectra of terephthalic acid solution under V–visible light illumination for B,N-TiO$_2$ samples: (a)B,N-TiO$_2$-650; (b) B,N-TiO$_2$-600; (c) B,N-TiO$_2$-550 and (d) B,N-TiO$_2$-500.

Secondly, the surface structure of B,N-TiO$_2$ had been changed with variable temperatures of nitrogen doping, which is shown in the XPS of Fig. 3. When the nitrogen-doping temperature is lower ($< 550\ ^{\circ}$C), the main forms of doped boron and nitrogen in the B,N-TiO$_2$ are Ti–O–B–N or Ti–O–N and Ti–O–B bonds. The Ti–O–B–N structure plays a vital role in photocatalytic activity in visible light. When the nitrogen doping temperature is higher ($> 600\ ^{\circ}$C), the Ti–O–B–N structure is unstable and then transforms into Ti–O–B or Ti–B and Ti–N bonds. Otherwise, the more Ti–N bonds are formed at higher temperature in ammonia atmosphere. Higher temperature also results in more oxygen vacancies. The transformation of surface structure is shown in Scheme 1. The analyses of EPR and XPS further confirm these results.

The 3d states of Ti^{3+} below the conduction band at ~ 1.2 eV, which are typically formed by trapping the electrons adjacent to the oxygen vacancy sites, can be considered as the color center responsible for its visible light absorption. However these sites can also act as electron-hole recombination centers, leading to the decrease in photocatalytic activity, which is in agreement with the previous studies [37,38]. The Ti^{3+} sites associated with oxygen vacancies are attributed to the recombination centers of the photoinduced electrons and holes. In our research, keeping the B content constant, the N content in the titania lattice increases with the doping temperatures, which leads to an increase in the concentration of oxygen vacancies. B,N-TiO$_2$-650 with the highest N dopant content has the most oxygen vacancies and Ti^{3+} species, EPR also supports this conclusion further. Furthermore, substitutional N atoms may cause additional Ti^{3+} species, so it is not surprising that B,N-TiO$_2$-650 exhibits hardly any photocatalytic activity under the visible light.

However under the UV–visible light, the main bulk TiO$_2$ can be excited in UV-light, which contributes to the photocatalytic activity. With B,N-TiO$_2$-550 as an example, the degradation ratio of MO for 30 min is 2.5% and 20% under visible and UV–vis light irradiation, respectively. Owing to the synergistic effect, the B,N-TiO$_2$-550 catalyst exhibits the highest photocatalytic activity under UV–vis light as well as under visible light. For B,N-TiO$_2$-650, its photocatalytic activity is higher than that of B,N-TiO$_2$-600, which can be attributed to the formation of mixed phases of anatase and rutile at higher annealing temperature. Many researches also presented that the formation of a small quantity of anatase and rutile phase on the titania surface can improve the photocatalytic activity [39,40].

4. Conclusions

In summary, B,N-codoped TiO$_2$ was prepared by B doping first and then nitrogen doping. The effect of the nitrogen doping temperature on the structure and photocatalytic activity of B,N-TiO$_2$ was investigated. The surface structures of boron and nitrogen co-doped TiO$_2$ were analyzed based on XPS spectra of B 1s, N 1s, O 1s and Ti 2p. The results suggested that the boron and nitrogen can be incorporated into the TiO$_2$ lattice either interstitially or substitutionally or both, and the Ti–O–B–N structure plays a vital role in photocatalytic activity under visible light. The photocatalytic activity of B,N-TiO$_2$ increases with the increase of the nitrogen doping temperatures at first and then decreases with the further increase of the temperatures. The B,N-TiO$_2$-550 catalyst exhibits the highest photocatalytic activity under visible light and UV–visible light irradiation, which can be attributed to the synergistic effect of boron and nitrogen doping. But, too high nitrogen-doping temperature may cause many oxygen vacancies and Ti^{3+} species, resulting in the decrease of photocatalytic activity in visible light.

References

[1] R. Asahi, T. Morikawa, T. Ohwaki, K. Aoki, Y. Taga, Science 293 (2001) 269.
[2] D. Chen, D. Yang, Q. Wang, Z.Y. Jiang, Ind. Eng. Chem. Res. 45 (2006) 4110.
[3] C.K. Xu, S.U.M. Khan, Electrochem. Solid State Lett. 10 (2007) B56.
[4] J. Wang, D.N. Tafen, J.P. Lewis, Z.L. Hong, A. Manivannan, M.J. Zhi, M. Li, N.Q. Wu, J. Am. Chem. Soc. 131 (2009) 12290.
[5] W.K. Ho, J.C. Yu, S.C. Lee, J. Solid State Chem. 179 (2006) 1171.
[6] D.G. Huang, S.J. Liao, J.M. Liu, Z. Dang, L. Petrik, J. Photochem. Photobiol. Chem. 184 (2006) 282.
[7] M.K. Lee, T.H. Shih, J. Electrochem. Soc. 154 (2007) 49.
[8] H.Y. Liu, L. Gao, J. Am. Chem. Soc. 87 (2004) 1582.
[9] J.G. Yu, M.H. Zhou, B. Cheng, X.J. Zhao, J. Mol. Catal. A Chem. 246 (2006) 176.
[10] J. Yang, H.Z. Bai, X.C. Tan, J.S. Lian, Appl. Surf. Sci. 253 (2006) 1988.
[11] S. Yin, M. Komatsu, Q.W. Zhang, F. Saito, T. Sato, J. Mater. Sci. 42 (2007) 2399.
[12] C.C. Pan, J.C.S. Wu, Mater. Chem. Phys. 100 (2006) 102.
[13] L. Zhou, X. Tan, L. Zhao, M. Sun, Coll. Czech., Chem. Commun. 72 (2007) 379.
[14] H. Ozaki, S. Iwamoto, M. Inoue, Catal. Lett. 113 (2007) 95.
[15] S. In, A. Oriov, R. Berg, F. Garcia, S. Pedrosa-Jimenez, M.S. Tikhov, D.S. Wright, R.M. Lambert, J. Am. Chem. Soc. 129 (2007) 13790.
[16] G. Liu, Y.N. Zhao, C.H. Sun, F. Li, G.Q. Lu, H.M. Cheng, Angew. Chem. Int. Ed. 47 (2008) 4516.
[17] G. Liu, C.H. Sun, L.N. Cheng, Y.G. Jin, H.F. Lu, L.Z. Wang, S.C. Smith, G.Q. Lu, H.M. Cheng, J. Phys. Chem. C 113 (2009) 12317.
[18] P. Chen, W. Li, T.L. Zhou, Y.P. Jin, M.Y. Gu, J. Photochem. Photobiol. A Chem. 168 (2004) 97.
[19] T.J. Mason, J.P. Lorimer, D.M. Bates, Y. Zhao, Ultrason. Sonochem. 1 (1994) S91.
[20] T. Hirakawa, Y. Nosaka, Langmuir 18 (2002) 3247.
[21] N. Lu, H.M. Zhao, J.Y. Li, X. Quan, S. Chen, Sep. Purif. Technol. 62 (2008) 668.
[22] S. Sugai, H. Watanabe, T. Kioka, H. Miki, K. Kawasaki, Surf. Sci. 259 (1991) 109.
[23] D.R. Rainer, S.M. Vesecky, M. Koranne, W.S. Oh, D.W. Goodman, J. Catal. 167 (1997) 234.
[24] J.A. Rodriguez, T. Jirsak, J. Dvorak, S. Sambasivan, D. Fischer, J. Phys. Chem. B 104 (2000) 319.

Scheme 1. The transformation of surface structures of B,N-TiO$_2$.

[25] E. Gyorgy, A. Perez del Pino, P. Serra, J.L. Morenza, Surf. Coat. Technol. 173 (2003) 265.
[26] X.B. Chen, C. Burda, J. Phys. Chem. B 108 (2004) 15446.
[27] M.S. Wong, H.P. Chou, T.S. Yang, Thin Solid Films 494 (2006) 244.
[28] S. Sakthivel, M. Janczarek, H. Kisch, J. Phys. Chem. B 108 (2004) 19384.
[29] M. Sathish, B. Viswanathan, R.P. Viswanath, C.S. Gopinath, Chem. Mater. 17 (2005) 6349.
[31] F. Peng, L.F. Cai, H. Yu, H.J. Wang, J. Yang, J. Solid State Chem. 181 (2008) 130.
[32] S. Livraghi, M.R. Chierotti, E. Giamello, J. Phys. Chem. C 112 (2008) 17244.
[33] N.O. Gopal, H.H. Lo, S.C. Ke, J. Am. Chem. Soc. 130 (2008) 2760.

[34] Y. Sakatani, J. Nunoshige, H. Ando, K. Okusako, H. Koike, T. Takata, J.N. Kondo, M. Hara, K. Domen, Chem. Lett. 32 (2003) 1156.
[35] H. Irie, Y. Watanabe, K. Hashimoto, J. Phys. Chem. B 107 (2003) 5483.
[36] N. Serpone, J. Phys. Chem. B 110 (2006) 24287.
[37] S. Takeda, S. Suzuki, H. Odaka, H. Hosono, Thin Solid Films 392 (2001) 338.
[38] S. Ikeda, N. Sugiyama, S. Murakami, H. Kominami, Y. Kera, H. Noguchi, K. Uosaki, T. Torimoto, B. Ohtani, Phys. Chem. Chem. Phys. 5 (2003) 778.
[39] M. Yan, F. Chen, J. Zhang, M. Anpo, J. Phys. Chem. B 109 (2005) 8673.
[40] D. Gumy, C. Morais, P. Bowen, C. Pulgarin, S. Giraldo, R. Hajdu, J. Kiwi, Appl. Catal. B 63 (2006) 76.